Global Biogeochemical Cycles

RESEARCH ARTICLE
10.1029/2019GB006236

Nutrient Controls on Export Production in the Southern Ocean

Lionel A. Arteaga[1], Markus Pahlow[2], Seth M. Bushinsky[1], and Jorge L. Sarmiento[1]

[1]Program in Atmospheric and Oceanic Sciences, Princeton University, Princeton, NJ, USA, [2]GEOMAR Helmholtz Centre for Ocean Research Kiel, Kiel, Germany

Key Points:
- Organic carbon export is inferred from float-based observations of mesopelagic oxygen and surface nitrate drawdown in the Southern Ocean
- Our estimates agree with previous observations showing an increase in inferred export in the vicinity of the polar front
- We hypothesize that iron limitation enhances silicification by diatoms, thereby increasing the ballasting effect of biogenic carbon export

Supporting Information:
- Supporting Information S1

Correspondence to:
L. A. Arteaga,
laaq@princeton.edu

Citation:
Arteaga, L. A., Pahlow, M., Bushinsky, S. M., & Sarmiento, J. L. (2019). Nutrient controls on export production in the Southern Ocean. *Global Biogeochemical Cycles*, *33*, 942–956. https://doi.org/10.1029/2019GB006236

Received 1 APR 2019
Accepted 24 JUN 2019
Accepted article online 4 JUL 2019
Published online 5 AUG 2019

Abstract We use observations from novel biogeochemical profiling floats deployed by the Southern Ocean Carbon and Climate Observations and Modeling program to estimate annual net community production (ANCP; associated with carbon export) from the seasonal drawdown of mesopelagic oxygen and surface nitrate in the Southern Ocean. Our estimates agree with previous observations in showing an increase in ANCP in the vicinity of the polar front (~3 mol C m^{-2} y^{-1}), compared to lower rates in the subtropical zone (≤ 1 mol C m^{-2} y^{-1}) and the seasonal ice zone (<2 mol C m^{-2} y^{-1}). Paradoxically, the increase in ANCP south of the subtropical front is associated with elevated surface nitrate and silicate concentrations, but decreasing surface iron. We hypothesize that iron limitation promotes silicification in diatoms, which is evidenced by the low silicate to nitrate ratio of surface waters around the Antarctic polar front. High diatom silicification increases the ballasting effect of particulate organic carbon and overall ANCP in this region. A model-based assessment of our methods shows a good agreement between ANCP estimates based on oxygen and nitrate drawdown and the modeled downward organic carbon flux at 100 m. This agreement supports the presumption that net biological consumption is the dominant process affecting the drawdown of these chemical tracers and that, given sufficient data, ANCP can be inferred from observations of oxygen and/or nitrate drawdown in the Southern Ocean.

1. Introduction

The Southern Ocean is a region of major biogeochemical relevance, associated with strong air-sea fluxes of carbon dioxide (CO_2) (Gruber et al., 2009) and linked to the regulation of Earth's climate through changes in the efficiency of nutrient utilization by phytoplankton and associated carbon export (Sigman & Boyle, 2000). Biological carbon export in the Southern Ocean, driven largely by the sinking of biogenic particles, has been estimated to account for about 30% of the global annual carbon export (~10 Pg C yr^{-1}, globally; Arteaga et al., 2018; Schlitzer, 2002). The efficiency and magnitude of organic carbon export in this region has implications not only for local marine biogeochemistry, but also for the supply of nutrients that sustain about three quarters of the biological production north of 30°S (Sarmiento et al., 2004).

In the Southern Ocean, biological productivity is limited primarily by nitrate (NO_3) in the subtropical zone (STZ), north of the subtropical front (STF) (~40°S) (Arteaga et al., 2014; Moore et al., 2013). South of 40°S, iron (Fe) is considered the main limiting nutrient of phytoplankton growth (Boyd et al., 2007; Martin et al., 1990; Moore et al., 2013). Despite the evidence for strong iron limitation, large diatom blooms occur in Southern Ocean waters (Brzezinski et al., 2001; Quéguiner et al., 1997), and sediment trap studies show large opal fluxes beneath these blooms (Honjo et al., 2000). Diatoms constitute a large fraction of the autotrophic biomass in the Southern Ocean, particularly in the vicinity of the polar front (PF) (~ 50°S) (Balch et al., 2016; Rosengard et al., 2015). This phytoplankton group is characterized by a silica cell wall (opal), which makes them potentially denser than the fluid around them and promotes their sinking toward deeper sections of the water column (Miklasz & Denny, 2010; Smayda, 1970). Diatoms thrive in environments with sufficient silicic acid, such as the Southern Ocean (Sarmiento et al., 2004), necessary for the development of the silica shell (Brzezinski, 1985; Tréguer et al., 2018).

Diatoms are associated with high rates of organic carbon export (Smetacek, 1999) and are estimated to account for up to 40% of global marine primary production and particulate organic carbon (POC) export (Jin et al., 2006; Nelson et al., 1995). However, opal-rich sediments, located below areas of high diatom-driven particle flux such as south of the PF in the Southern Ocean, show a low content of organic carbon compared

with calcite-dominated minerals north of the PF (Seiter et al., 2004b). This suggests that organic matter exported and originated from diatom blooms has a relatively low transfer efficiency of carbon to sediments, in the bathypelagic layer (below 1,000 m; Henson et al., 2012), with most of the organic matter being remineralized in the mesopelagic zone (roughly between 100 and 1,000 m). If this is the case, the production and subsequent remineralization of organic carbon should be evident in the seasonal drawdown of nutrients (e.g., nitrate) in the upper productive layer, as well as in the seasonal drawdown of dissolved oxygen (O_2) during the respiration of the sinking organic matter in the mesopelagic zone.

Argo floats equipped with biogeochemical sensors provide a novel opportunity to evaluate marine biogeochemical and ecosystem dynamics. Specifically, autonomous profiling floats deployed by the Southern Ocean Carbon and Climate Observations and Modeling (SOCCOM) program are equipped with nitrate and oxygen sensors that allow the estimation of seasonal rates of net community production (NCP). NCP represents the net production of organic carbon after accounting for the respiration needs of the autotrophic and heterotrophic components of the ecosystem (Ducklow & Doney, 2013) and should be equivalent to organic carbon export under steady-state conditions (i.e., no net accumulation of organic carbon in the upper ocean). In the Southern Ocean (defined as the oceanic region south of 30°S), the mesopelagic zone undergoes a seasonal cycle of ventilation and respiration: During winter mixing, mesopelagic oxygen levels are restored to atmospheric levels. This is followed by a shallowing of the mixed layer above the *community* compensation depth (depth at which gross organic matter production is equivalent to community respiration) in the spring–summer period, during which (mesopelagic) oxygen is consumed via respiration of sinking organic matter (Najjar & Keeling, 1997). Based on this seasonality in oxygen levels, respiration rates have been estimated from the temporal evolution of oxygen measured by autonomous profiling floats in the Southern Ocean (Martz et al., 2008), as well as other ocean regions (Hennon et al., 2016; Riser & Johnson, 2008). Similarly, the net production of organic matter can be assessed from the seasonal drawdown of the upper ocean nitrate reservoir (Johnson et al., 2017). In this study, we build upon these ideas to estimate annual net community production (ANCP) based on the seasonal drawdown of surface nitrate and mesopelagic oxygen, using data obtained from 123 profiling floats deployed by the SOCCOM program. We compare and combine our results with previous estimates of ANCP for the Southern Ocean, showing a consistent pattern of increased NCP in the vicinity of the Antarctic PF. We relate this pattern to meridional trends in surface nutrients, particularly Fe, silicate (Si), and NO_3, suggesting an increase in carbon export driven by a high Si utilization and silicification due to enhanced iron limitation south of the STF (~ 40°S). Finally, we use a coupled physical and biogeochemical ocean model to assess the capacity of seasonal trends in mesopelagic dissolved oxygen and surface nitrate to represent the magnitude and spatial patterns of marine carbon export in the Southern Ocean.

2. Methods

2.1. Float Data

We use data from 123 biogeochemical profiling floats deployed by the SOCCOM program between 2013 and 2018. The floats are equipped with conductivity-temperature-depth (CTD), oxygen, nitrate, pH, and bio-optical sensors. Quality-controlled float data were obtained from the SOCCOM data portal (http://soccompu.princeton.edu/www/index.html; Johnson et al., 2018). Detailed float data processing and quality control information is provided in Johnson et al. (2017). The temporal sampling resolution of the floats varies between 5 and 10 days (with most floats sampling every 10 days). The vertical resolution of the measurements taken by the floats varies with depth, with measurements every 5 m in the upper 100 m (uppermost sampled depth is ~ 5 or 7 m below surface). Vertical sampling resolution decreases to 10 m below 100-m depth, 20 m below 360-m depth, and 50 m between 400- and 2,000-m depth. Vertical profiles are smoothed using a seven-point running-median filter. Data flagged as "questionable" or "bad" are not considered in our analysis.

2.2. Oxygen-Based Estimation of ANCP

The floats perform air-calibrated, fluorescence-based measurements of dissolved oxygen in the water column (μmol kg^{-1}) (Johnson et al., 2017). The evolution of the oxygen concentration in time is affected by physical advection and diffusivity, as well as the balance between local biological production and respiration (J_{O_2}):

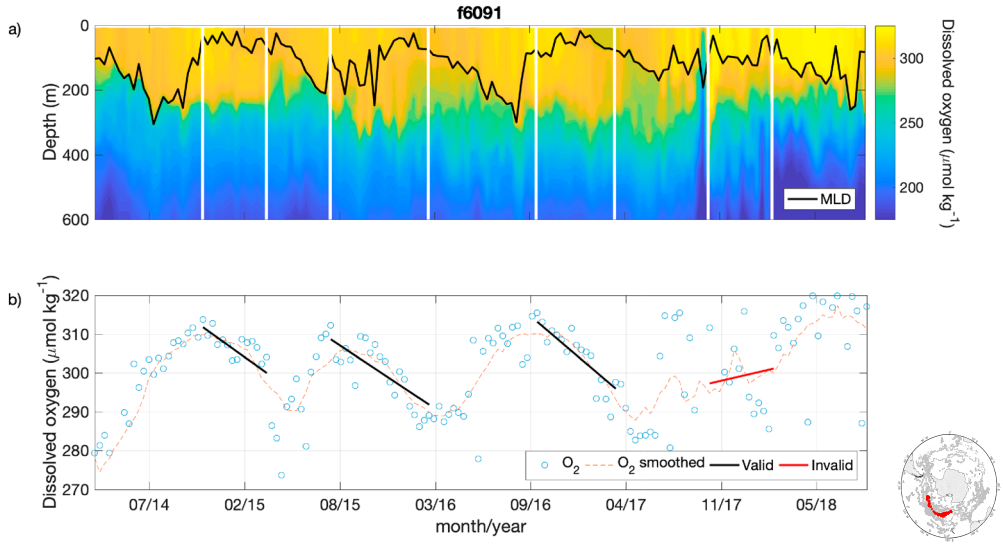

Figure 1. (a) Vertical profiles of dissolved oxygen sampled between 2014 and 2018 by SOCCOM float 6091. Continuous black line represents the MLD. Vertical white lines encompass the period of late winter maximum and spring–summer minimum in mean oxygen concentration during which NCP is estimated. (b) Temporal evolution of dissolved oxygen at 150 m measured by float 6091. Blue open circles show the oxygen measurements of each float profile, while the dashed orange line represents the smoothed oxygen signal from a 10-point moving mean filter. Black (valid) lines show the linear fit to the smoothed oxygen signal used to infer NCP from oxygen drawdown. The red line shows a seasonal period over which ΔS at 500 m is larger than 0.05 psu, and thus this seasonal period is considered "invalid" and discarded for the estimation of NCP. Map on the bottom right corner shows in red the displacement of float 6091 in the Southern Ocean (trajectories in gray are for all float profiles available in the present SOCCOM data set).
SOCCOM = Southern Ocean Carbon and Climate Observations and Modeling; MLD = depth of the mixed layer; NCP = net community production.

$$\frac{\mathrm{d}[\mathrm{O}_2]}{\mathrm{d}t} = -\vec{u}\cdot\nabla[\mathrm{O}_2] + \nabla\cdot(D\cdot\nabla[\mathrm{O}_2]) + J_{\mathrm{O}_2} \tag{1}$$

where $\vec{u}$ denotes the velocity field, ∇ denotes the gradient operator in three dimensions, and D denotes the eddy diffusivity tensor. Below the community compensation depth (depth of $J_{\mathrm{O}_2} = 0$), the net (biological) change of oxygen in time is determined by the remineralization (respiration (R)) of organic carbon produced in the upper productive layer:

$$\frac{\mathrm{d}[\mathrm{O}_2]}{\mathrm{d}t} = -\vec{u}\cdot\nabla[\mathrm{O}_2] + \nabla\cdot(D\cdot\nabla[\mathrm{O}_2]) - R \tag{2}$$

Based on the studies of Najjar and Keeling (1997) and Hennon et al. (2016), we make the presumption that given a large float array, positive and negative gradients in oxygen concentration driven by water mass changes tend to cancel out. Thus, in order to infer rates of organic matter remineralization in the mesopelagic zone, we assume that the advective and diffusive terms in equation (2) play a negligible role for the temporal evolution of mesopelagic oxygen levels during the biologically productive season in the Southern Ocean (see section 3.5 for a model-based assessment of our methods):

$$R(z) = -0.69\frac{\text{mol C}}{\text{mol O}_2}\times\frac{\mathrm{d}[\mathrm{O}_2(z)]}{\mathrm{d}t} \tag{3}$$

where the factor of 0.69 represents the respiratory quotient for organic-matter remineralization ($\frac{117\text{ mol C}}{170\text{ mol O}_2}$; Anderson & Sarmiento, 1994). A running 10-point mean filter is applied to the temporal evolution of oxygen at each depth level in order to smooth large fluctuations in O_2 concentration. R at each depth is inferred from the slope of a linear regression fitted to the smoothed temporal evolution of oxygen ($\frac{\mathrm{d}[\mathrm{O}_2]}{\mathrm{d}t}$) during the productive period of the year (Figure 1) and converted to carbon units using the respiratory quotient. Annual cycles of mesopelagic oxygen are analyzed to find the late winter maximum (August–November) and spring–summer minimum (January–March) mean oxygen concentration between 100 and 200 m. The productive period is defined as the section of the annual cycle between the beginning of the late winter maximum month and the end of the summer minimum month. We expect most of the oceanic export production

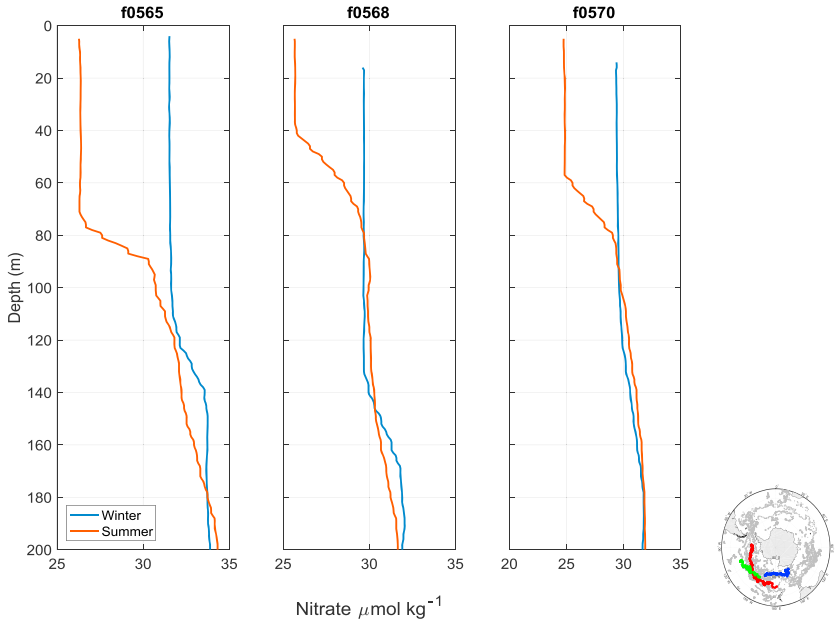

Figure 2. Winter maximum and summer minimum nitrate profiles for SOCCOM floats 0565, 0568, and 0570. Each profile represents the mean of the winter (summer) month of maximum (minimum) mean nitrate in the upper 200 m, used to infer annual net community production. Map on the bottom right corner shows the displacement of the floats in the Southern Ocean (red = f0565, blue = f0568, and green = f0570). Trajectories in gray are for all float profiles available in the present SOCCOM data set. SOCCOM = Southern Ocean Carbon and Climate Observations and Modeling.

to occur during this period, although minor export events could also occur during fall and winter months. In an effort to detect float periods where $\frac{d[O_2]}{dt}$ is not driven mainly by biological respiration, we remove periods following the same criteria as in the analysis of seasonal nitrate drawdown carried out by Johnson et al. (2017): If the change in salinity (ΔS) at 500 m from winter to summer is > 0.05, if the float moved > 8° in longitude, or if the float moved > 5° in latitude. Finally, we estimate ANCP as depth-integrated respiration between 100 and 500 m, multiplied by the number of days of the productive period of each float (D_{prod}):

$$\text{ANCP} = \int_{100}^{500} R(z)dz \times D_{prod} \quad (4)$$

The upper boundary of the vertical integration was selected based on preliminary analyses showing that most of the primary productivity as well as the spring–summer depth of the mixed layer are constrained to above 100 m. The mixed layer depth (MLD) is calculated using float in situ temperature and salinity profiles following de Boyer Montégut et al. (2004). Remineralization estimates approach 0 at about 400-m depth (supporting information Figure S1). Therefore, we constrain the bottom depth of integration to 500 m. Due to the nature of our method, negative estimates of ANCP can occur and are indeed present in our analysis. These estimates are not removed in order to avoid inducing a bias in ANCP estimates. However, we do remove outliers from both ends of the ANCP estimates distribution (i.e., positive and negative ends) identified through a box plot and located beyond ~ the 5th and 95th data percentiles. After removing outliers and float periods potentially not driven by biological respiration, we obtain a total of 98 ANCP estimates based on the analysis of mesopelagic oxygen drawdown (Table S1).

2.3. Nitrate-Based Estimation of ANCP

SOCCOM floats collect ultraviolet-based measurements of nitrate in the water column (μmol kg^{-1}). Contrary to oxygen, nitrate concentrations are not affected by air-sea fluxes, thus simplifying the interpretation of nitrate changes in the upper ocean, where most of the biological production occurs. The change of the nitrate concentration in time ($\frac{d[NO_3]}{dt}$) is controlled by the same physical and biological processes that affect oxygen (equation (1)). Here we infer ANCP from the annual drawdown in the surface nitrate reservoir (upper 200 m; Figure 2). Similarly as for oxygen, we identify the late winter maximum month and the spring–summer minimum month in mean nitrate concentration in the upper 200 m. The winter and summer nitrate concentrations are obtained as the means of all profiles in the winter maximum month and the summer minimum

month, respectively. ANCP is estimated as the vertical integral from the surface to 200 m of the decrease in the winter-summer nitrate concentration, converted to carbon units using a Redfield ratio of $\frac{106\ \text{mol C}}{16\ \text{mol NO}_3}$ (≈ 6.6).

$$\text{ANCP} = 6.6 \times \int_{\text{surface}}^{200} \text{NO}_3^{\text{winter}}(z) - \text{NO}_3^{\text{summer}}(z) \quad \text{d}z \tag{5}$$

We filter nitrate-based ANCP estimates by applying the same criteria as for our oxygen-based estimates, based on winter to summer changes in salinity at 500 m, the total zonal and meridional float displacement, and removal of outliers at both tails of the distribution of ANCP estimates. After removing outliers and float periods potentially not driven by biological nitrogen consumption, we obtain a total of 81 ANCP estimates based on the analysis of surface nitrate drawdown (Table S2). The accuracy of the seasonal drawdown of nitrate in representing ANCP is also constrained by the assumption that net biological productivity plays a major role over advective and diffusive processes in determining the temporal change of surface nitrate in the Southern Ocean. We address the validity of our oxygen- and nitrate-based method in capturing ANCP within a model framework in section 3.5.

2.4. Nutrient and Sediment Data

We complement float data with nutrient information on surface Si (μmol kg^{-1}) obtained from a global gridded monthly climatology with a 1° by 1° spatial resolution (World Ocean Atlas 2013 [WOA13]; Garcia et al., 2014), downloaded from https://www.nodc.noaa.gov/OC5/woa13/. The gridded Si product is interpolated from sparse climatological observations. Both products (interpolated and noninterpolated) show similar latitudinal trends. The gridded and interpolated Si climatology is subsampled in the same geographical location and month of the float profiles. Fe information is obtained from an updated (June 2015) version of a global database of dissolved iron observations (Tagliabue et al., 2012; available at https://www.bodc.ac.uk/geotraces/data/historical/). Fe observations are scarce and not gridded. Scattered Fe observations are subsampled by averaging all available observations in the upper 200 m proximate to each float profile within a horizontal radius of 500 m. In order to account for the seasonality in the Fe database while maximizing the amount of retrieved information, Fe observations are only subsampled if they were taken within 4 months of the corresponding float profile (without taking into consideration the exact date [year] in which the Fe observation was taken).

Meridional patterns of inferred carbon export are compared with information from 1° by 1° gridded data sets of opal and calcite content in sediments (wt%) (Seiter et al., 2004a) obtained from https://doi.pangaea.de/10.1594/PANGAEA.251593. Inferred deep carbon flux to sediments based on the diffusive oxygen flux across the sediment-water interface (Seiter et al., 2005) is also analyzed and obtained from https://doi.pangaea.de/10.1594/PANGAEA.251594. Gridded sediment climatologies are subsampled according to the geographical location of the float profiles. Subsampled nutrient and sediment data according to float profiles yield a total of 8,997 observations (total number of profiles in the float data set). Latitudinal patterns of nutrient and sediment data are smoothed by applying a 200-point moving mean filter in order to enhance the meridional trends.

2.5. POC Sinking and Air-Sea CO_2 Flux Estimates

Estimates of ANCP in four different environmental zones of the Southern Ocean (see section 3.1) are compared with observations of POC flux obtained from a global compilation of sediment trap and ^{234}Th measurements (Mouw et al., 2016). Meridional patterns of inferred Southern Ocean carbon export are compared with zonally averaged mean annual and summer air-sea CO_2 fluxes obtained for 2014–2015 using a neural network interpolation method based on shipboard CO_2 measurements (Landschützer et al., 2017). The neural network utilizes a two-step approach. In the first step, the ocean is subdivided into 16 biomes using a self-organizing map with inputs of monthly 1° × 1° sea surface temperature, sea surface salinity, climatological MLD, and a pCO_2 climatology (Takahashi et al., 2009). These biomes shift monthly to establish regions of similar surface properties throughout the year. In the second step, a feed-forward network establishes relationships for each biome between observations of surface ocean pCO_2 with inputs of sea surface temperature, sea surface salinity, climatological MLD, chlorophyll, and atmospheric pCO_2, producing global maps of surface ocean pCO_2 based on those relationships.

2.6. Model Output

We test the consistency of our methods in reproducing carbon export within a model framework using output from a physical ocean model with a 1° nominal grid (CM2-1°; Griffies et al., 2015) coupled with a marine

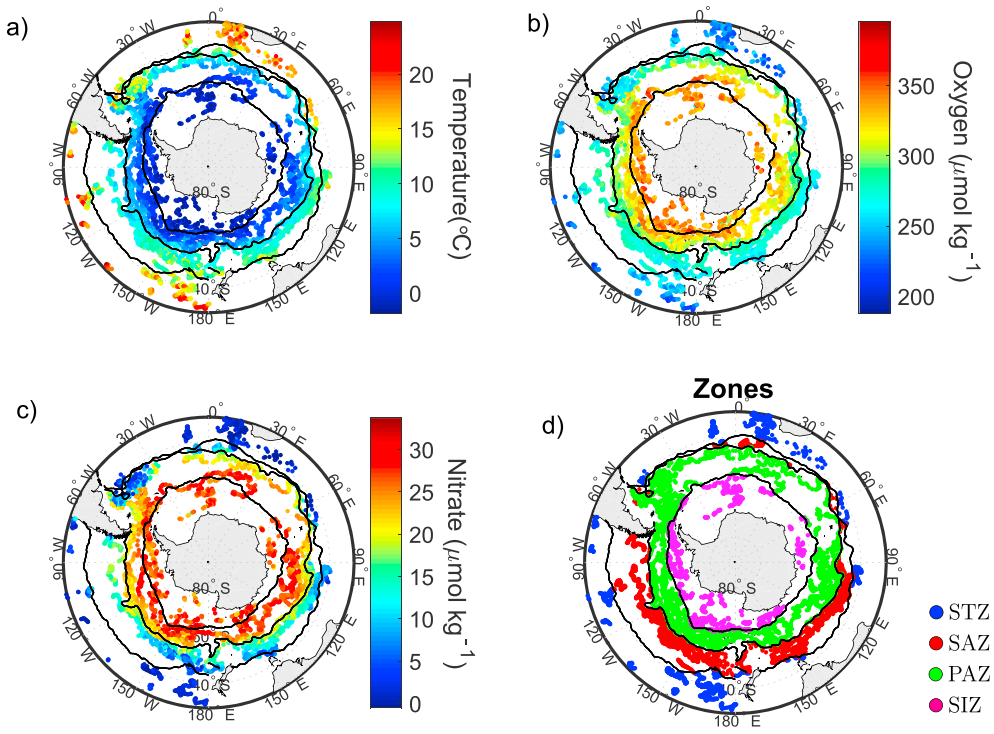

Figure 3. Mean mixed layer (a) temperature, (b) oxygen, and (c) nitrate, and location of the Southern Ocean frontal zones defined in this study. (d) The fronts divide the Southern Ocean into four major zones, indicated by the color of the positions of the floats profiles: subtropical zone (STZ, blue), subantarctic zone (SAZ, red), polar Antarctic zone (PAZ, green), seasonal ice zone (SIZ, magenta). The subtropical front (STF) separates the STZ and the SAZ. The polar front (PF) divides the SAZ and the PAZ, and the seasonal ice front (SIF) defines the extent of the SIZ.

biogeochemical model of high complexity (TOPAZ; Dunne et al., 2010), simulated under natural climate conditions (no anthropogenic climate forcing). We use an annual climatology, representative of the mean state of the model biogeochemical variables. Dissolved oxygen outputs are obtained with a 5-day temporal resolution, while nitrate is obtained as monthly means, allowing a close representation of our methodology within the model framework.

We employ two different approaches to evaluate the capacity of our methods in reproducing patterns of ANCP (analogous to carbon export) in the Southern Ocean: (a) We locate the month of late winter oxygen (nitrate) maximum and spring–summer minimum in each model grid, and estimate ANCP based on the seasonal trend in mesopelagic oxygen drawdown over this period (integrated between 100 and 500 m). ANCP is also estimated based on the drawdown of the oceanic nitrate reservoir in the upper 200 m at each model grid. (b) We superimpose the trajectories from our SOCCOM floats on the model grid and subsample the model oxygen concentration along these trajectories over a similar seasonal period as the float data. ANCP is estimated from the seasonal oxygen drawdown along the float-based model trajectories (integrated between 100 and 500 m). For nitrate, we subsample the model at the month and position of the float's late winter maximum and summer minimum and estimate ANCP from the drawdown of the nitrate reservoir in the upper 200 m. Assessment (a) provides an estimate of how well ANCP can be inferred from local observations of oxygen and nitrate drawdown, assuming a complete spatial and temporal coverage of oceanic data. Assessment (b) provides a more direct comparison of our method in retrieving spatial patterns of ANCP, taking into account the drifting nature of the floats.

3. Results and Discussion

3.1. Environmental Zones

We relate meridional patterns of ANCP and associated carbon export to the mean position of the major environmental fronts in the Southern Ocean (Orsi et al., 1995) computed by Bushinsky et al. (2017), based on a mean 2004–2014 Argo-based climatology of temperature and salinity (Roemmich & Gilson, 2009; Figure 3). The STF separates the STZ and the subantarctic zone (SAZ). The PF divides the SAZ and the polar Antarctic

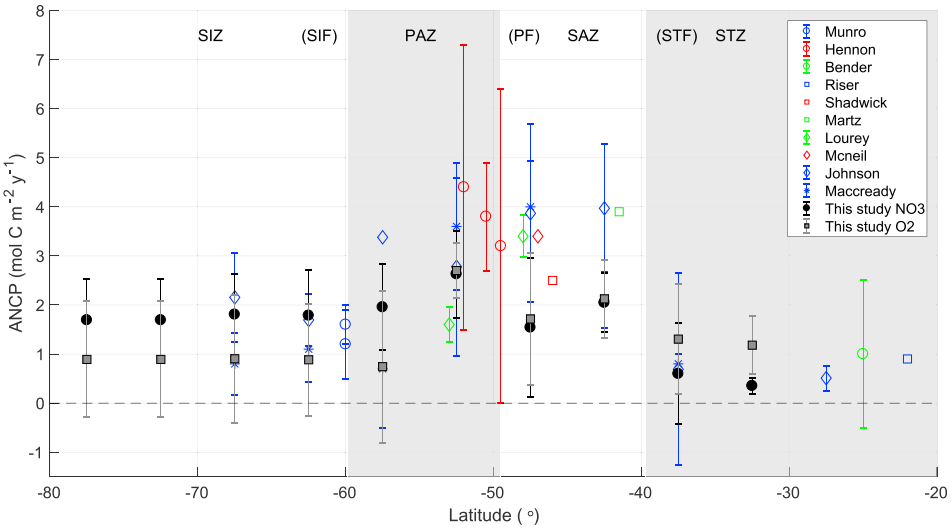

Figure 4. Meridional pattern of ANCP estimates (and associated errors) in the Southern Ocean from previous studies (Bender & Jönsson, 2016; Johnson et al., 2017; Hennon et al., 2016; Lourey & Trull, 2001; MacCready & Quay, 2001; Martz et al., 2008; McNeil & Tilbrook, 2009; Munro et al., 2015; Shadwick et al., 2015; Riser & Johnson, 2008) and from our analysis of nitrate (black filled circles) and oxygen (gray filled squares) drawdown measured by Southern Ocean Carbon and Climate Observations and Modeling floats. ANCP estimates from this study are inferred from 5° latitudinally binned estimates (± standard deviation). White and gray-shaded backgrounds represent the four environmental regions: subtropical zone (STZ), subantarctic zone (SAZ), polar Antarctic zone (PAZ), and the seasonal ice zone (SIZ). Environmental fronts constraining these regions are indicated in brackets: subtropical front (STF), polar front (PF), and the front delimiting the extent of the seasonal ice zone (SIF). Number of single ANCP estimates based on nitrate (oxygen) for each latitudinal bin (± 2.5° latitude): 32.5°S = 4 (4), 37.5°S = 6 (11), 42.5°S = 5 (6), 47.5°S = 11 (16), 52.5°S = 9 (7), 57.5°S = 8 (14), 62.5°S = 20 (22), 67.5°S = 13 (13), 72.5°S = 5 (5), 77.5°S = 5 (5). ANCP = annual net community production.

zone (PAZ), and the seasonal ice front (SIF) defines the extent of the seasonal ice zone (SIZ). Surface mixed layer properties measured by the floats show clear latitudinal patterns across the zones delimited by the oceanic fronts: Temperature decreases from > 15 °C in the STZ to ~ 10 °C in the SAZ and < 5 °C toward the SIZ. Mean oxygen in the mixed layer increases from < 250 μmol O_2 kg^{-1} in the STZ to ~ 270 μmol O_2 kg^{-1} in the SAZ, and > 300 μmol O_2 kg^{-1} south of the PF. Nitrate also shows a meridional increase from < 5 μmol NO_3 kg^{-1} in the STZ to > 10 μmol NO_3 kg^{-1} in the SAZ and > 20 μmol NO_3 kg^{-1} south of the PF.

3.2. Estimates of ANCP

We infer general latitudinal patterns of ANCP by grouping our oxygen- and nitrate-based estimates in 5° latitudinal bands (Figure 4). Both estimates are highest in the PAZ and SAZ. Oxgen-based estimates of ANCP are lowest in the SIZ, while nitrate-based estimates are lowest in the STZ. Except for the STZ, oxygen-based ANCP estimates are lower than nitrate-based estimates, which may be due to some important fraction of organic carbon remineralization occurring above 100 m south of the STF and therefore missed in our oxygen-based estimation of ANCP. The general latitudinal trend of our estimates is similar to that inferred from a compilation of previous observations based on oxygen drawdown (Hennon et al., 2016; Martz et al., 2008; Riser & Johnson, 2008), as well as on changes in nutrients, dissolved inorganic carbon, and pCO_2 (Bender & Jönsson, 2016; Johnson et al., 2017; Lourey & Trull, 2001; MacCready & Quay, 2001; McNeil & Tilbrook, 2009; Munro et al., 2015; Shadwick et al., 2015). An important caveat of most of these estimates is that they have a large degree of uncertainty, which prevents us from obtaining clear statistical differences between zones. This is likely due to the inherent difficulty in the quantification of biologically driven rates and fluxes in the ocean. In section 3.5 we show that despite the large uncertainties, general patterns of export production in the Southern Ocean can be represented by the mean seasonal drawdown in mesopelagic oxygen and surface nitrate. Overall, in situ-based estimates for the Southern Ocean show a consistent pattern of low ANCP in the STZ (≤ 1 mol C m^{-2} y^{-1}), highest toward the PF (≥ 3 mol C m^{-2} y^{-1}), and intermediate to low in the SIZ (< 2 mol C m^{-2} y^{-1}). The upper limit of Southern Ocean ANCP estimates is similar to that inferred for other oceanic regions (~ 4 mol C m^{-2} y^{-1}; Emerson, 2014).

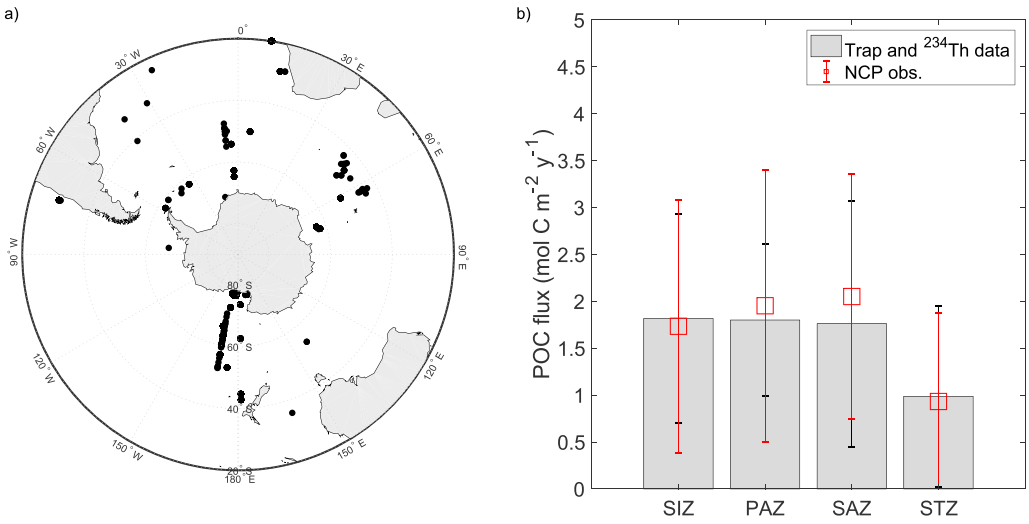

Figure 5. (a) Locations of available particle flux data from sediment traps and ^{234}Th in the Southern Ocean (Mouw et al., 2016). (b) Comparison of binned mesopelagic POC flux ($Flux_{100m}$-$Flux_{1000m}$) from sediment trap and ^{234}Th data and averaged NCP estimates for the four environmental regions in the Southern Ocean (± standard deviation). Values shown in panel (b) for particle-based flux (and NCP estimates) are as follows: STZ = 0.9 ± 0.9 (0.9 ± 0.9); SAZ = 1.8 ± 1.3 (2 ± 1.3); PAZ = 1.8 ± 0.8 (1.9 ± 1.4); SIZ = 1.8 ± 1.1 (1.7 ± 1.3). POC = particulate organic carbon; NCP = net community production; STZ = subtropical zone; SAZ = subantarctic zone; PAZ = polar Antarctic zone; SIZ = seasonal ice zone.

3.3. Comparison With Particle Flux Data

Assuming that organic carbon produced via photosynthesis does not accumulate in the upper ocean (steady-state conditions), and that most of it is exported in the form of particles and aerobically remineralized in the mesopelagic zone, annual estimates of mesopelagic POC flux and ANCP from surface nutrient and mesopelagic oxygen drawdown should converge. We subsampled all available POC flux information south of 20°S from a global compilation of sediment trap and ^{234}Th measurements (Mouw et al., 2016), and compute mesopelagic POC flux to compare against all ANCP estimates compiled in Figure 4. Particle flux observations in the Southern Ocean are scarce (Figure 5a). Hence, we binned and averaged the compiled POC flux data and ANCP estimates into four regions representing the main environmental zones of the Southern Ocean (STZ, SAZ, PAZ, and SIZ). Observations of POC flux are also binned and averaged into depth intervals of 100 m between 100 and 1,000 m. The observation-based POC flux over the mesopelagic zone is computed as the difference in POC flux between 100 and 1,000 m, which is the depth range where we expect most of the remineralization to occur (Honjo et al., 2000). Annual POC flux is inferred from daily estimates by assuming a steady mean flux over a period of 180 days. The mean POC flux from sediment trap and ^{234}Th measurements shows a similar latitudinal pattern of low surface flux in the STZ and higher flux in the other (poleward) regions (Figure 5b). The mean flux inferred from ANCP estimates agrees well within the uncertainty of combined trap and ^{234}Th measurements, with a slightly larger flux inferred for the PAZ and SAZ. The slight bias toward lower values in the POC flux data at the PAZ and SAZ may be associated with well-documented issues with trap hydrodynamics, zooplankton interaction, and solubilization of material, preventing the settling and conservation of particles in the trap (Baker et al., 1988; Buesseler, 1991; 2007; Kähler & Bauerfeind, 2001). Particle-based methods such as sediment traps and analysis of ^{234}Th also ignore the contribution of labile dissolved organic carbon (DOC) production to the total organic carbon pool. However, DOC production is generally considered to be low in the Southern Ocean (< 20%; Carlson et al., 1998; Hansell & Carlson, 1998), with the exception of one model-based study which found the contribution of downward flux of DOC to be significant in the top 500 m of the water column (Schlitzer, 2002). Overall, particle-based observations tend to be lower (~50%) than modeled fluxes constrained by hydrographic oxygen, nutrient, and carbon data (Schlitzer et al., 2003; Usbeck et al., 2003). However, given the large uncertainty in both POC flux and ANCP estimates, it is difficult to identify any particular mechanism or error source responsible for the slight disagreement between flux estimates.

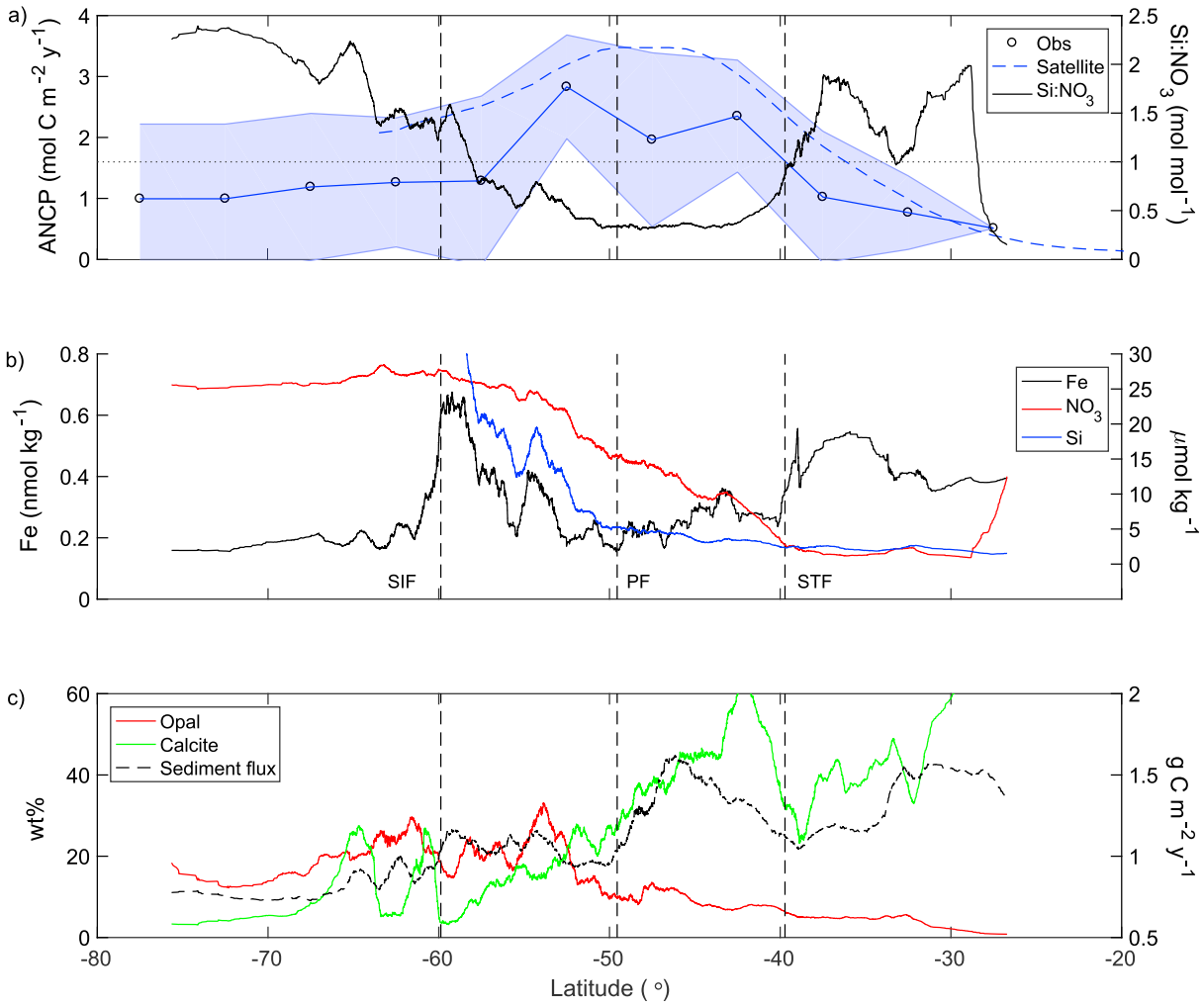

Figure 6. (a; *Y* axis left) Meridional pattern of ANCP estimates presented in Figure 1, calculated as the mean (± standard deviation) of 5° latitudinal bins (blue line with circles and shaded area), and satellite-based carbon export estimates from Arteaga et al., 2018 (blue dashed line). (*Y* axis right) Silicate to nitrate ($Si:NO_3$) ratio obtained from float nitrate measurements in the mixed layer and surface WOA13 silicate climatology subsampled at the same location and month as the float profiles (black continuous line). Grey dotted line shows a $Si:NO_3$ = 1 mol mol^{-1}, characteristic of nutrient-replete diatoms (Brzezinski, 1985). (b; *Y* axis left) Dissolved iron (Fe) concentration subsampled in relation to the floats positions (black line). (*Y* axis right) Nitrate (red line) and silicate (blue line) concentrations obtained as indicated above. (c; *Y* axis left) Weight percentage of opal (red line) and calcite (green line) in sediments (Seiter et al., 2004b). (*Y* axis right) Annual POC flux to sediments (black dashed line; Seiter et al., 2005). Sediment climatologies are sampled in the same location as float profiles. Nutrient and sediment latitudinal patterns have been smoothed by applying a 200-point moving mean filter. ANCP = annual net community production.

3.4. Nutrient Controls on Carbon Export

ANCP estimates (Figure 4) are compiled and averaged in 5° latitudinal bins. The mean meridional trend of ANCP increases south of the STF (~ 40°S), associated with an increase in the surface concentration of nitrate and silicate (Figure 6). The STF marks the transition from nitrate-limited to nitrate-replete conditions for phytoplankton growth (Arteaga et al., 2014; Moore et al., 2013). Paradoxically, the increase in ANCP estimates also occurs over an area of the Southern Ocean where the surface iron concentration decreases to its lowest values (Figure 6b). We explain this paradoxical pattern by analyzing the meridional trend in the dissolved silicate to nitrate ratio ($Si:NO_3$) and revising the effects of iron limitation on phytoplankton stoichiometry.

The increase in surface NO_3 and Si is driven by the upwelling of Circumpolar Deep Water around the Antarctic PF (Sarmiento et al., 2004). Upwelled water north of the PF is transported equatorward by the formation of Subantarctic Mode Water, which injects nutrients into the subtropical thermocline. As water is transported northward, nitrate and silicate are stripped from the surface ocean through biological export production.

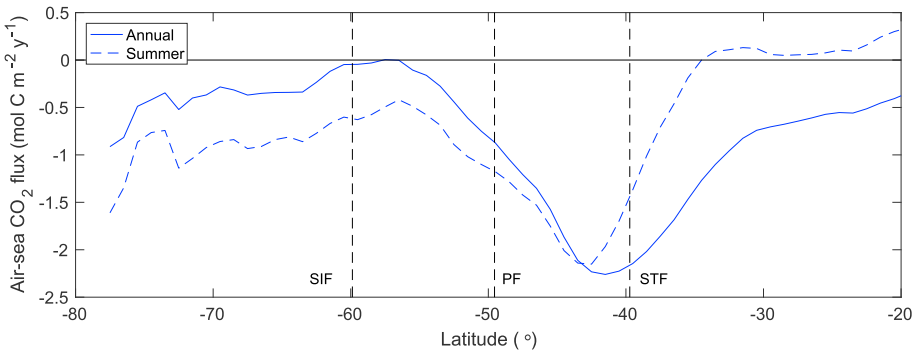

Figure 7. Mean 2014–2015 annual and summer (continuous and dashed blue lines, respectively) zonally averaged air-sea flux of CO_2 computed from the Landschützer et al. (2017) neural network interpolation method. The summer annual flux is computed based on the average monthly CO_2 flux obtained from January to April. Positive (negative) values denote CO_2 flux out of (into) the ocean. The black horizontal line shows the transition from ocean CO_2 outgassing (positive flux) to ocean uptake (negative flux). SIF = seasonal ice front; PF = polar front; STF = subtropical front.

The supply Si:NO_3 ratio of upwelled waters near the PF is ~ 2:1 (mol mol^{-1}) (Gordon & Molinelli, 1986). Under nutrient-replete conditions, diatoms take up Si and NO_3 in a 1:1 molar ratio (Brzezinski, 1985). Thus, we would expect nitrate to be depleted before silicic acid (Brzezinski et al., 2003). However, the observed pattern is the opposite, with NO_3 concentrations >10 μmol kg^{-1} and Si <5 μmol kg^{-} north of the upwelling region, between the PF and the STF (Figure 6b). The difference between surface nitrate and silicate depletion can be inferred from the surface Si:NO_3 ratio: The Si:NO_3 ratio is lowest (<1 mol mol^{-1}) in the vicinity of the PF, beneath the region of highest ANCP (associated to carbon export) constrained between the STF and SIF, and increases south toward the Antarctic and north toward the STZ (Figure 6a).

The preferential depletion of silicate with respect to nitrate is likely caused by the effect of iron limitation on the stoichiometry of the POC exported to the deep ocean. Several studies have shown that under iron-limiting conditions, diatoms exhibit preferential net uptake of Si with respect to NO_3 (Hutchins & Bruland, 1998; Takeda, 1998), leading to a significant increase in diatom Si:NO_3 ratio, from 1 (mol mol^{-1}) under nutrient-replete conditions, to 4–6 times higher (Franck et al., 2000). This is the same range as the difference between the diatom Si:NO_3 uptake ratio under nutrient-replete conditions (1 mol mol^{-1}) and the minimum observed around the PF (Si:NO_3 ~ 0.3 [mol mol^{-1}]). Iron limitation impedes cellular nitrogen assimilation (Brzezinski et al., 2003; Hutchins & Bruland, 1998; Takeda, 1998) leading to nitrogen limitation of phytoplankton growth. We hypothesize that low iron concentrations in the vicinity of the PF lead to enhanced silicification of diatoms, reflected in the low Si:NO_3 ratio of the surface water, thereby increasing the ballasting effect of POC and overall ANCP in this region. A similar mechanism of enhanced silica burial and carbon export induced by iron limiting conditions has been proposed for oceanic upwelling margins (Brzezinski et al., 2015; Pichevin et al., 2014). The meridional pattern of ANCP agrees well with a recent satellite-based estimate of export production for the Southern Ocean (Arteaga et al., 2018; Figure 6a). This estimate is based on an export efficiency model constrained by a positive relationship between export efficiency and phytoplankton Si utilization in the Southern Ocean (Britten et al., 2017).

The general meridional distribution of inferred ANCP and carbon export agrees well with patterns of high diatom productivity in the Southern Ocean (Balch et al., 2016; Rosengard et al., 2015). Recent in situ flux observations carried out during two research cruises across the Southern Ocean found that POC export out of the euphotic zone correlates well with the export of biogenic silicate (BSi) (Rosengard et al., 2015). That study suggests that diatom-rich communities induce high export of labile POC aggregates, which can drive the high rates of remineralization in the mesopelagic zone inferred from our analysis of oxygen drawdown. Conversely, communities with smaller calcifying phytoplankton induce less POC export and with lower lability, which results in lower mesopelagic remineralization and greater transfer efficiency of organic carbon to the bathypelagic zone (Rosengard et al., 2015). Sediment analyses show distinct mineral accumulation across the Southern Ocean, with opal-dominated minerals increasing south toward the SIF (Figure 6c). Calcite-dominated sediments show an opposite pattern, increasing north toward the STZ. Estimates of the amount of POC that reaches the sea floor also increase northward, correspondingly with calcite and oppo-

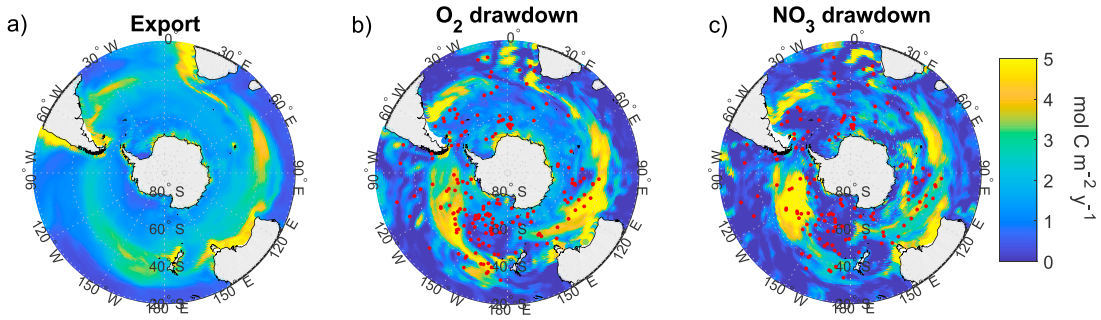

Figure 8. Export production in CM2-1° estimated from (a) downward flux of detritus-associated organic carbon at 100 m, (b) the seasonal mesopelagic oxygen drawdown at each model grid, and (c) the seasonal surface nitrate drawdown at each model grid. Red dots in (b) and (c) indicate the mean position of the Southern Ocean Carbon and Climate Observations and Modeling float trajectories superimposed on the model grid cell, used to estimate annual net community production from model oxygen and nitrate outputs extracted from the drifting float trajectories.

site to the trend of opal-dominated sediments. This suggests a larger transfer efficiency of organic carbon by calcite minerals relative to opal (Figure 6c) (Seiter et al., 2005).

The zonally averaged mean annual ocean CO_2 flux for 2014–2015 calculated using the Landschützer et al. (2017) neural network interpolation of shipboard CO_2 measurements shows a similar meridional trend to that of ANCP estimates (Figure 7). The flux of CO_2 into the ocean increases south of 30°S and is highest ~42°S. South of the PF, oceanic CO_2 uptake decreases, with a neutral flux near the SIF and moderate uptake further south. We compute a mean annual flux for summer only, using the average CO_2 flux obtained from January through April (Figure 7). In the summer, the highest rate of CO_2 uptake is slightly further south than the annual mean, with stronger uptake everywhere south of the PF. The observed contemporary CO_2 flux is a combination of natural fluxes driven by biology and physics, with the anthropogenic flux into the ocean overlaid. The natural carbon cycle in the Southern Ocean is typically thought to be a balance of upwelling-driven outgassing in the south near the PF and uptake to the north as subtropical waters move south and cool, increasing their solubility (Gruber et al., 2019). The colocation of the highest inferred ANCP and CO_2 uptake suggests an important role for biological export in setting the location and magnitude of the peak uptake. Further analysis is required to separate the physical and biological components of the observed CO_2 flux, especially to account for the delay between biological production and CO_2 flux induced by slow gas exchange.

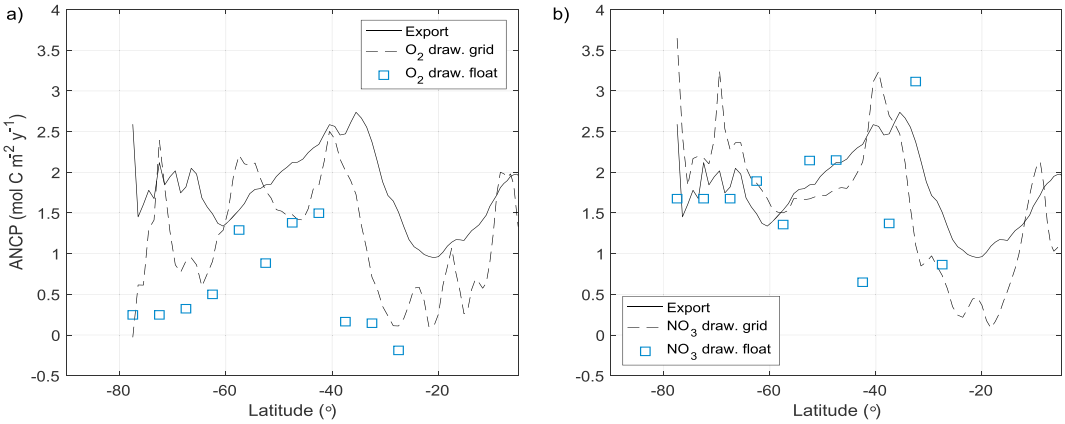

Figure 9. Meridional trend of ANCP in CM2-1° estimated from the downward flux of detritus-associated organic carbon at 100 m (continuous black line in a and b) and the seasonal drawdown of (a) oxygen and (b) nitrate. Dashed lines show the zonal mean ANCP by assessing the seasonal drawdown at each model grid cell. Open blue squares show estimates obtained from averaging 5° latitudinal bins of ANCP inferred by superimposing float trajectories on the model grid and measuring the drawdown in model oxygen and nitrate outputs extracted from drifting float trajectories. ANCP = annual net community production.

Table 1
Coefficient of Variation (Standard Deviation:Mean) of Binned ANCP Estimates for Each 5° Latitudinal Band Obtained From Float and Model Data Based on the Seasonal Drawdown of Mesopelagic Oxygen (O_2-Based) and Surface Nitrate (NO_3-Based)

	O_2-based			NO_3-based		
Latitude	Float CV	Model CV	Method error (%)	Float CV	Model CV	Method error (%)
−27.5	—	5.4	112.8	—	3.4	41.4
−32.5	0.5	64	93.8	0.5	1.7	34.1
−37.5	0.9	19.7	93.6	1.7	2.2	46.6
−42.5	0.4	1.3	37.3	0.3	7.5	72.8
−47.5	0.8	2.5	34.2	0.9	2.2	2.6
−52.5	0.2	4.4	52.2	0.3	0.9	16.1
−57.5	2.1	2.4	16.7	0.4	1.2	12.4
−62.5	1.3	5.5	66.5	0.5	0.5	26.8
−67.5	1.4	6	83.2	0.5	0.9	12.8
−72.5	1.3	7.7	86.8	0.5	0.9	10.5
Mean	1	10.8	67.7	0.6	2.1	27.6

Note. Also shown are the errors of binned ANCP estimates from model O_2 and NO_3 drawdown with respect to the downward flux of detritus-associated organic carbon at 100 m (method error). ANCP = annual net community production; CV = coefficient of variation.

3.5. Model-Based Assessment of ANCP Estimates From Oxygen and Nitrate Drawdown

A major assumption of our methods to estimate ANCP from the seasonal drawdown in oxygen and nitrate is that the advective and diffusive terms in equation (1) (and similarly for nitrate) are negligible. In order to test the validity of our assumptions, we apply our methods within a model framework by (a) assessing seasonal oxygen and nitrate changes (drawdown) at each model grid cell, and (b) by assessing the drawdown in model oxygen and nitrate output sampled along the same trajectory and seasonal period of the floats analyzed in this study. The methodology applied to obtain ANCP estimates from oxygen and nitrate is similar as for the float data (see section 2.6 for model and methods details).

We compare oxygen- and nitrate-based estimates of ANCP at each model grid cell (model assessment (a)) with the flux of detritus-associated organic carbon at 100 m in the model (Figure 8). Our methods capture the main spatial patterns of carbon flux in the model. Both methods (oxygen- and nitrate-based) accentuate export patterns in regions of high detritus flux and temper export in regions of low flux. The nitrate-based method reproduces better the overall mean meridional variability in inferred ANCP than the oxygen-based approach (Figure 9b). Estimates of ANCP based on the analysis of model oxygen drawdown from superimposed float trajectories, averaged in 5° latitudinal bins (model assessment (b)), underestimate the meridional trend in carbon export (Figure 9a). This may be caused by the fact that the mean positions of the superimposed float trajectories are located in regions of low modeled detritus flux (red dots in Figure 8b). Binned estimates of ANCP based on model oxygen and nitrate outputs show coefficients of variation (the ratio of standard deivation:mean) larger than those obtained from binned float-based estimates (Table 1). Despite this large variability, the analysis of model oxygen and nitrate drawdown based on float trajectories is able to estimate the model detritus flux within 68% and 28%, respectively (Table 1). This is in line with a recent assessment of ANCP estimates based on nitrate drawdown within a model framework, which diagnosed the potential error of ignoring physical transport to be within 20% (Johnson et al., 2017). The agreement between model-based nitrate drawdown and carbon fluxes south of 25°S supports the presumption that nitrate drawdown is primarily caused by net biological consumption and that estimates of ANCP can be inferred from such an analysis. As observed in the gridded model output (Figure 8), the large uncertainty associated with inferred ANCP from nitrate and oxygen drawdown might represent the natural spatial variability of carbon export in the Southern Ocean.

The analysis of mesopelagic signals is hindered by the potential decrease in the signal-to-noise ratio of biological rates of oxygen consumption with respect to physical tranport of dissolved oxygen. However, based on our model assessment, we believe that our oxygen-based method can at the very least provide qualitative observations of the meridional variability of carbon export in the Southern Ocean. This is particularly true

in oceanic regions with large seasonal changes in oxygen, where the remineralization signal-to-noise ratio is maximized. The meridional pattern of the detritus-associated organic carbon flux in the model is similar to that of in situ-based ANCP estimates. The highest flux of organic carbon in the model occurs north of 40°S, further north than in the ANCP estimates. While our goal is not to validate the model's biogeochemical component, it is likely that the occurrence of highest organic export fluxes north of 40°S is due to a relatively simple dependence of export production on net primary production in the model (Arteaga et al., 2018), which does not take into consideration more complex processes affecting export production in the Southern Ocean (such as enhanced silicification promoted by iron limitation).

4. Conclusions

We use observations from novel biogeochemical profiling floats deployed by the SOCCOM program to estimate ANCP (associated with carbon export) from the seasonal drawdown of mesopelagic oxygen and surface nitrate in the Southern Ocean. Our estimates agree with previous observations in showing an increase in ANCP in the vicinity of the PF (~ 3 mol C m^{-2} y^{-1}), compared to lower rates in the STZ (≤ 1 mol C m^{-2} y^{-1}) and the seasonal ice zone (< 2 mol C m^{-2} y^{-1}). We hypothesize that iron limitation induced by very low iron concentrations south of the STZ leads to enhanced silicification of diatoms, reflected in the low Si:NO_3 ratio of the surface water, thereby increasing the ballasting effect of POC and overall ANCP in this region. The overall meridional pattern of ANCP in the Southern Ocean is similar to that of the zonally averaged annual mean ocean CO_2 flux inferred from a neural network interpolation method (Landschützer et al., 2017). The colocation of the highest inferred ANCP and CO_2 uptake suggests an important role for biological export in setting the location and magnitude of the peak uptake. However, further analysis is required to separate the physical and biological components of the observed CO_2 flux, especially to account for the delay between biological production and CO_2 flux induced by slow gas exchange.

Our methods rely on the presumption that given sufficient data, advective and diffusive processes may be considered negligible in order to infer broad biologically driven changes of chemical tracers. We assess the validity of using trends of mesopelagic oxygen and surface nitrate drawdown to estimate carbon export fluxes within a model framework. Overall, the analysis of model mesopelagic oxygen and surface nitrate drawdown replicates well the spatial pattern of modeled downward organic carbon flux at 100 m. This agreement supports the presumption that net biological consumption is the dominant process affecting the drawdown of these chemical tracers and that given sufficient data, ANCP can be inferred from observations of oxygen and/or nitrate drawdown in the Southern Ocean.

Acknowledgments
We would like to thank the many people at the Monterey Bay Aquarium Research Institute, the University of Washington, and the University of Maine who quality controlled and corrected the SOCCOM float data. SOCCOM float data were collected and made freely available by the Southern Ocean Carbon and Climate Observations and Modeling (SOCCOM) Project funded by the National Science Foundation, Division of Polar Programs (NSF PLR-1425989), supplemented by NOAA and NASA (PI Jorge Sarmiento). L. Arteaga is mainly supported by NASA under Award NNX17AI73G. S. M. Bushinsky is supported by the SOCCOM project, NASA (NNX17AI73G), and the Carbon Mitigation Initiative (CMI) project sponsored by BP at Princeton University. M. Pahlow was supported by Deutsche Forschungsgemeinschaft (DFG) project SFB754 (Sonderforschungsbereich 754 "Climate-Biogeochemistry Interactions in the Tropical Ocean," www.sfb754.de). We would also like to thank Rick Slater for providing CM2-1° output to evaluate our methodology. All details and web addresses needed to access the data used to produce our results are described in section 2 of this paper.

References

Anderson, L. A., & Sarmiento, J. L. (1994). Redfield ratios of remineralization determined by nutrient data analysis. *Global Biogeochemical Cycles*, *8*, 65–80. https://doi.org/10.1029/93GB03318

Arteaga, L., Haeëntjens, N., Boss, E., Johnson, K. S., & Sarmiento, J. L. (2018). Assessment of export efficiency equations in the Southern Ocean applied to satellite-based net primary production. *Journal of Geophysical Research: Oceans*, *123*, 2945–2964. https://doi.org/10.1002/2018JC013787

Arteaga, L., Pahlow, M., & Oschlies, A. (2014). Global patterns of phytoplankton nutrient and light colimitation inferred from an optimality-based model. *Global Biogeochemical Cycles*, *28*, 648–661. https://doi.org/10.1002/2013GB004668

Baker, E. T., Milburn, H. B., & Tennant, D. A. (1988). Field assessment of sediment trap efficiency under varying flow conditions. *Journal of Marine Research*, *46*(3), 573–592. https://doi.org/doi:10.1357/002224088785113522

Balch, W. M., Bates, N. R., Lam, P. J., Twining, B. S., Rosengard, S. Z., Bowler, B. C., et al. (2016). Factors regulating the Great Calcite Belt in the Southern Ocean and its biogeochemical significance. *Global Biogeochemical Cycles*, *30*, 1124–1144. https://doi.org/10.1002/2016GB005414

Bender, M. L., & Jönsson, B. (2016). Is seasonal net community production in the South Pacific Subtropical Gyre anomalously low? *Geophysical Research Letters*, *43*, 9757–9763. https://doi.org/10.1002/2016GL070220

Boyd, P. W., Jickells, T., Law, C. S., Blain, S., Boyle, E. A., Buesseler, K. O., et al. (2007). Mesoscale iron enrichment experiments 1993–2005: Synthesis and future directions. *Science*, *315*, 612–617. https://doi.org/10.1126/science.1131669

Britten, G. L., Wakamatsu, L., & Primeau, F. W. (2017). The temperature-ballast hypothesis explains carbon export efficiency observations in the Southern Ocean. *Geophysical Research Letters*, *44*, 1831–1838. https://doi.org/10.1002/2016GL072378

Brzezinski, M. A. (1985). The Si:C:N ratio of marine diatoms: Interspecific variability and the effect of some environmental variables. *Journal of Phycology*, *21*(3), 347–357. https://doi.org/10.1111/j.0022-3646.1985.00347.x

Brzezinski, M. A., Dickson, M. L., Nelson, D. M., & Sambrotto, R. (2003). Ratios of Si, C and N uptake by microplankton in the Southern Ocean. *Deep Sea Research Part II: Topical Studies in Oceanography*, *50*(3), 619–633. https://doi.org/10.1016/S0967-0645(02)00587-8

Brzezinski, M. A., Krause, J. W., Bundy, R. M., Barbeau, K. A., Franks, P., Goericke, R., et al. (2015). Enhanced silica ballasting from iron stress sustains carbon export in a frontal zone within the California Current. *Journal of Geophysical Research: Oceans*, *120*, 4654–4669. https://doi.org/10.1002/2015JC010829

Brzezinski, M. A., Nelson, D. M., Franck, V. M., & Sigmon, D. E. (2001). Silicon dynamics within an intense open-ocean diatom bloom in the Pacific sector of the Southern Ocean. *Deep Sea Research Part II: Topical Studies in Oceanography*, *48*(19), 3997–4018. https://doi.org/10.1016/S0967-0645(01)00078-9

Buesseler, K. O. (1991). Do upper-ocean sediment traps provide an accurate record of particle flux? *Nature*, *353*, 420–423. https://doi.org/10.1038/353420a0

Buesseler, K. O., Antia, A. N., Chen, M., Fowler, S. W., Gardner, W. D., Gustafsson, O., et al. (2007). An assessment of the use of sediment traps for estimating upper ocean particle fluxes. *Journal of Marine Research*, *65*(3), 345–416. https://doi.org/doi:10.1357/002224007781567621

Bushinsky, S. M., Gray, A. R., Johnson, K. S., & Sarmiento, J. L. (2017). Oxygen in the Southern Ocean from argo floats: Determination of processes driving air-sea fluxes. *Journal of Geophysical Research: Oceans*, *122*, 8661–8682. https://doi.org/10.1002/2017JC012923

Carlson, C. A., Ducklow, H. W., Hansell, D. A., & Smith, W. O. (1998). Organic carbon partitioning during spring phytoplankton blooms in the Ross Sea polynya and the Sargasso Sea. *Limnology and Oceanography*, *43*(3), 375–386. https://doi.org/10.4319/lo.1998.43.3.0375

de Boyer Montégut, C., Madec, G., Fischer, A. S., Lazar, A., & Iudicone, D. (2004). Mixed layer depth over the global ocean: An examination of profile data and a profile-based climatology. *Journal of Geophysical Research*, *109*, C12003. https://doi.org/10.1029/2004JC002378

Ducklow, H. W., & Doney, S. C. (2013). What is the metabolic state of the oligotrophic ocean? A debate. *Annual Review of Marine Science*, *5*(1), 525–533. https://doi.org/10.1146/annurev-marine-121211-172331

Dunne, J. P., Gnanadesikan, A., Sarmiento, J. L., & Slater, R. (2010). Technical description of the prototype version (v0) of Tracers of Phytoplankton with Allometric Zooplankton (TOPAZ) ocean biogeochemical model as used in the Princeton IFMIP model. *Biogeosciences*, *7*, 3593–3624. https://doi.org/10.5194/bg-7-3593-2010

Emerson, S. (2014). Annual net community production and the biological carbon flux in the ocean. *Global Biogeochemical Cycles*, *28*, 14–28. https://doi.org/10.1002/2013GB004680

Franck, V. M., Brzezinski, M. A., Coale, K. H., & Nelson, D. M. (2000). Iron and silicic acid concentrations regulate Si uptake north and south of the Polar Frontal Zone in the Pacific sector of the Southern Ocean. *Deep Sea Research Part II: Topical Studies in Oceanography*, *47*(15), 3315–3338. https://doi.org/10.1016/S0967-0645(00)00070-9

Garcia, H. E., Locarnini, R. A., Boyer, T. P., Antonov, J. I., Baranova, O. K., Zweng, M. M., Reagan, J. R., & Johnson, D. R. (2014). World Ocean Atlas 2013. Vol. 4: Dissolved Inorganic Nutrients (phosphate, nitrate, silicate). In S. Levitus, A. Mishonov, Technical Ed., NOAA Atlas NESDIS76, (25 pp.)

Gordon, A., & Molinelli, E. (1986). Thermohaline and chemical distributions and the atlas data set. In A. Gordon (Ed.), *Southern Ocean atlas* (pp. 3–233). New York: Columbia University Press.

Griffies, S. M., Winton, M., Anderson, W. G., Benson, R., Delworth, T. L., Dufour, C. O., et al. (2015). Impacts on ocean heat from transient mesoscale eddies in a hierarchy of climate models. *Journal of Climate*, *28*(3), 952–977. https://doi.org/10.1175/JCLI-D-14-00353.1

Gruber, N., Gloor, M., Mikaloff Fletcher, S. E., Doney, S. C., Dutkiewicz, S., Follows, M. J., et al. (2009). Oceanic sources, sinks, and transport of atmospheric CO_2. *Global Biogeochemical Cycles*, *23*, GB1005. https://doi.org/10.1029/2008GB003349

Gruber, N., Landschtzer, P., & Lovenduski, N. S. (2019). The variable Southern Ocean carbon sink. *Annual Review of Marine Science*, *11*(1), 159–186. https://doi.org/10.1146/annurev-marine-121916-063407

Hansell, D. A., & Carlson, C. A. (1998). Net community production of dissolved organic carbon. *Global Biogeochemical Cycles*, *12*, 443–453. https://doi.org/10.1029/98GB01928

Hennon, T. D., Riser, S. C., & Mecking, S. (2016). Profiling float-based observations of net respiration beneath the mixed layer. *Global Biogeochemical Cycles*, *30*, 920–932. https://doi.org/10.1002/2016GB005380

Henson, S. A., Sanders, R., & Madsen, E. (2012). Global patterns in efficiency of particulate organic carbon export and transfer to the deep ocean. *Global Biogeochemical Cycles*, *26*, GB1028. https://doi.org/10.1029/2011GB004099

Honjo, S., Francois, R., Manganini, S., Dymond, J., & Collier, R. (2000). Particle fluxes to the interior of the Southern Ocean in the western Pacific sector along 170°W. *Deep Sea Research Part II: Topical Studies in Oceanography*, *47*(15–16), 3521–3548. https://doi.org/10.1016/s0967-0645(00)00077-1

Hutchins, D. A., & Bruland, K. W. (1998). Iron-limited diatom growth and Si:N uptake ratios in a coastal upwelling regime. *Nature*, *393*, 561–564. https://doi.org/10.1038/31203

Jin, X., Gruber, N., Dunne, J. P., Sarmiento, J. L., & Armstrong, R. A. (2006). Diagnosing the contribution of phytoplankton functional groups to the production and export of particulate organic carbon, $CaCO_3$, and opal from global nutrient and alkalinity distributions. *Global Biogeochemical Cycles*, *20*, GB2015. https://doi.org/10.1029/2005GB002532

Johnson, K. S., Plant, J. N., Coletti, L. J., Jannasch, H. W., Sakamoto, C. M., Riser, S. C., et al. (2017). Biogeochemical sensor performance in the SOCCOM profiling float array. *Journal of Geophysical Research: Oceans*, *122*, 6416–6436. https://doi.org/10.1002/2017jc012838

Johnson, K. S., Plant, J. N., Dunne, J. P., Talley, L. D., & Sarmiento, J. L. (2017). Annual nitrate drawdown observed by SOCCOM profiling floats and the relationship to annual net community production. *Journal of Geophysical Research: Oceans*, *122*, 6668–6683. https://doi.org/10.1002/2017jc012839

Johnson, K. S., Riser, S. C., Boss, E. S., Talley, L. D., Sarmiento, J. L., Swift, D. D., et al. (2018). SOCCOM foat data—Snapshot 2018-09-12. In *Southern Ocean Carbon and Climate Observations and Modeling (SOCCOM) float data archive*: UC San Diego Library Digital Collections. https://doi.org/10.6075/J0QJ7FJP

Kähler, P., & Bauerfeind, E. (2001). Organic particles in a shallow sediment trap: Substantial loss to the dissolved phase. *Limnology and Oceanography*, *46*(3), 719–723. https://doi.org/10.4319/lo.2001.46.3.0719

Landschützer, P., Gruber, N., & Bakker, D. C. E. (2017). An updated observation-based global monthly gridded sea surface pCO_2 and air-sea CO_2 flux product from 1982 through 2015 and its monthly climatology (NCEI accession 0160558). version 2.2., NOAA National Centers for Environmental Information. Dataset [2017-07-11]. Retrieved from https://www.nodc.noaa.gov/ocads/oceans/SPCO2_1982_2015_ETH_SOM_FFN.html

Lourey, M. J., & Trull, T. W. (2001). Seasonal nutrient depletion and carbon export in the Subantarctic and Polar Frontal zones of the Southern Ocean south of Australia. *Journal of Geophysical Research*, *106*(C12), 31463–31487. https://doi.org/10.1029/2000JC000287

MacCready, P., & Quay, P. (2001). Biological export flux in the Southern Ocean estimated from a climatological nitrate budget. *Deep Sea Research Part II: Topical Studies in Oceanography*, *48*(19), 4299–4322. https://doi.org/10.1016/S0967-0645(01)00090-X

Martin, J., Gordon, R. M., & Fitzwater, S. E. (1990). Iron in Antartic waters. *Nature*, *345*, 156–158. https://doi.org/10.1038/345156a0

Martz, T. R., Johnson, K. S., & Riser, S. C. (2008). Ocean metabolism observed with oxygen sensors on profiling floats in the South Pacific. *Limnology and Oceanography*, *53*(5part2), 2094–2111. https://doi.org/10.4319/lo.2008.53.5_part_2.2094

McNeil, B., & Tilbrook, B. (2009). A seasonal carbon budget for the sub-Antarctic Ocean, south of Australia. *Marine Chemistry*, *115*(3), 196–210. https://doi.org/10.1016/j.marchem.2009.08.006

Miklasz, K. A., & Denny, M. W. (2010). Diatom sinkings speeds: Improved predictions and insight from a modified Stokes' law. *Limnology and Oceanography*, *55*(6), 2513–2525. https://doi.org/10.4319/lo.2010.55.6.2513

Moore, C. M., Mills, M. M., Arrigo, K. R., Berman-Frank, I., Bopp, L., Boyd, P. W., et al. (2013). Processes and patterns of oceanic nutrient limitation. *Nature Geoscience*, *6*, 701–710. https://doi.org/10.1038/ngeo1765

Mouw, C. B., Barnett, A., McKinley, G. A., Gloege, L., & Pilcher, D. (2016). Global ocean particulate organic carbon flux merged with satellite parameters. *Earth System Science Data*, *8*(2), 531–541. https://doi.org/10.5194/essd-8-531-2016

Munro, D. R., Lovenduski, N. S., Stephens, B. B., Newberger, T., Arrigo, K. R., Takahashi, T., et al. (2015). Estimates of net community production in the Southern Ocean determined from time series observations (2002–2011) of nutrients, dissolved inorganic carbon, and surface ocean pCO_2 in Drake Passage. *Deep Sea Research Part II: Topical Studies in Oceanography*, *114*, 49–63. https://doi.org/10.1016/j.dsr2.2014.12.014

Najjar, R. G., & Keeling, R. F. (1997). Analysis of the mean annual cycle of the dissolved oxygen anomaly in the world ocean. *Journal of Marine Research*, *55*(1), 117–151. https://doi.org/10.1357/0022240973224481

Nelson, D. M., Tréguer, P., Brzezinski, M. A., Leynaert, A., & Quguiner, B. (1995). Production and dissolution of biogenic silica in the ocean: Revised global estimates, comparison with regional data and relationship to biogenic sedimentation. *Global Biogeochemical Cycles*, *9*(3), 359–372. https://doi.org/10.1029/95GB01070

Orsi, A. H., Whitworth, T., & Nowlin, W. D. (1995). On the meridional extent and fronts of the Antarctic Circumpolar Current. *Deep Sea Research Part I: Oceanographic Research Papers*, *42*(5), 641–673. https://doi.org/10.1016/0967-0637(95)00021-W

Pichevin, L. E., Ganeshram, R. S., Geibert, W., Thunell, R., & Hinton, R. (2014). Silica burial enhanced by iron limitation in oceanic upwelling margins. *Nature Geoscience*, *7*, 541–546. https://doi.org/10.1038/ngeo2181

Quéguiner, B., Tréguer, P., Peeken, I., & Scharek, R. (1997). Biogeochemical dynamics and the silicon cycle in the Atlantic sector of the Southern Ocean during austral spring 1992. *Deep Sea Research Part II: Topical Studies in Oceanography*, *44*(1–2), 69–89. https://doi.org/10.1016/s0967-0645(96)00066-5

Riser, S. C., & Johnson, K. S. (2008). Net production of oxygen in the subtropical ocean. *Nature*, *451*, 323–326. https://doi.org/10.1038/nature06441

Roemmich, D., & Gilson, J. (2009). The 2004–2008 mean and annual cycle of temperature, salinity, and steric height in the global ocean from the argo program. *Progress in Oceanography*, *82*(2), 81–100. https://doi.org/10.1016/j.pocean.2009.03.004

Rosengard, S. Z., Lam, P. J., Balch, W. M., Auro, M. E., Pike, S., Drapeau, D., & Bowler, B. (2015). Carbon export and transfer to depth across the Southern Ocean Great Calcite Belt. *Biogeosciences*, *12*(13), 3953–3971. https://doi.org/10.5194/bg-12-3953-2015

Sarmiento, J. L., Gruber, N., Brzezinski, M. A., & Dunne, J. P. (2004). High-latitude controls of thermocline nutrients and low latitude biological productivity. *Nature*, *427*, 56–60. https://doi.org/10.1038/nature02127

Schlitzer, R. (2002). Carbon export fluxes in the Southern Ocean: Results from inverse modeling and comparison with satellite-based estimates. *Deep Sea Research Part II: Topical Studies in Oceanography*, *49*(9), 1623–1644. https://doi.org/10.1016/S0967-0645(02)00004-8

Schlitzer, R., Usbeck, R., & Fischer, G. (2003). Inverse modeling of particulate organic carbon fluxes in the South Atlantic. In G. Wefer, S. Mulitza, & V. Ratmeyer (Eds.), *The South Atlantic in the late Quaternary: Reconstruction of material budgets and current systems*. Berlin Heidelberg: Springer. https://doi.org/10.1007/978-3-642-18917-3_1

Seiter, K., Hensen, C., Schröter, J., & Zabel, M. (2004a). Gridded data sets I [data set]. PANGAEA https://doi.org/10.1594/PANGAEA.251593 In supplement to: Seiter, K et al. (2004): Organic carbon content in surface sediments-defining regional provinces. *Deep Sea Research Part I: Oceanographic Research Papers*, *51*(12), 2001–2026. https://doi.org/10.1016/j.dsr.2004.06.014

Seiter, K., Hensen, C., Schröter, J., & Zabel, M. (2004b). Organic carbon content in surface sediments—Defining regional provinces. *Deep Sea Research Part I: Oceanographic Research Papers*, *51*(12), 2001–2026. https://doi.org/10.1016/j.dsr.2004.06.014

Seiter, K., Hensen, C., & Zabel, M. (2005). Benthic carbon mineralization on a global scale. *Global Biogeochemical Cycles*, *19*, GB1010. https://doi.org/10.1029/2004GB002225

Seiter, K., Hensen, C., & Zabel, M. (2005). Gridded data sets II [data set] PANGAEA https://doi.org/10.1594/PANGAEA.251594 In supplement to: Seiter, K et al. (2005): Benthic carbon mineralization on a global scale. *Global Biogeochemical Cycles*, *19*, GB1010. https://doi.org/10.1029/2004GB002225

Shadwick, E. H., Trull, T. W., Tilbrook, B., Sutton, A. J., Schulz, E., & Sabine, C. L. (2015). Seasonality of biological and physical controls on surface ocean CO_2 from hourly observations at the Southern Ocean Time Series site south of Australia. *Global Biogeochemical Cycles*, *29*, 223–238. https://doi.org/10.1002/2014GB004906

Sigman, D. M., & Boyle, E. A. (2000). Glacial/interglacial variations in atmospheric carbon dioxide. *Nature*, *407*(6806), 859–869. https://doi.org/10.1038/35038000

Smayda, T. J. (1970). The suspension and sinking of phytoplankton in the sea. *Oceanography Marine Biology: Annual Review*, *8*, 353–414.

Smetacek, V. (1999). Diatoms and the ocean carbon cycle. *Protist*, *150*(1), 25–32. https://doi.org/10.1016/S1434-4610(99)70006-4

Tagliabue, A., Mtshali, T., Aumont, O., Bowie, A. R., Klunder, M. B., Roychoudhury, A. N., & Swart, S. (2012). A global compilation of dissolved iron measurements: Focus on distributions and processes in the Southern Ocean. *Biogeosciences*, *9*(6), 2333–2349. https://doi.org/10.5194/bg-9-2333-2012

Takahashi, T., Sutherland, S. C., Wanninkhof, R., Sweeney, C., Feely, R. A., Chipman, D. W., et al. (2009). Climatological mean and decadal change in surface ocean pCO_2, and net sea-air CO_2 flux over the global oceans. *Deep Sea Research Part II: Topical Studies in Oceanography*, *56*(8), 554–577. https://doi.org/10.1016/j.dsr2.2008.12.009

Takeda, S. (1998). Influence of iron availability on nutrient consumption ratio of diatoms in oceanic waters. *Nature*, *393*(6), 774–777. https://doi.org/10.1038/31674

Tréguer, P., Bowler, C., Moriceau, B., Dutkiewicz, S., Gehlen, M., Aumont, O., et al. (2018). Influence of diatom diversity on the ocean biological carbon pump. *Nature Geoscience*, *11*(1), 27–37. https://doi.org/10.1038/s41561-017-0028-x

Usbeck, R., Schlitzer, R., Fischer, G., & Wefer, G. (2003). Particle fluxes in the ocean: Comparison of sediment trap data with results from inverse modeling. *Journal of Marine Systems*, *39*(3), 167–183. https://doi.org/10.1016/S0924-7963(03)00029-0